Published in final edited form as:

Environ Sci Technol. 2015 July 7; 49(13): 8067–8077. doi:10.1021/acs.est.5b01389.

Metabolomics Reveals that Aryl Hydrocarbon Receptor Activation by Environmental Chemicals Induces Systemic Metabolic Dysfunction in Mice

Limin Zhang[†,‡], **Emmanuel Hatzakis**[§], **Robert G. Nichols**[†], **Ruixin Hao**[†], **Jared Correll**[†], **Philip B. Smith**[&], **Christopher R. Chiaro**[†], **Gary H. Perdew**[†], and **Andrew D. Patterson**[†,*]

[†]Center for Molecular Toxicology and Carcinogenesis, Department of Veterinary and Biomedical Sciences, The Pennsylvania State University, University Park, Pennsylvania, 16802, USA

[‡]CAS Key Laboratory of Magnetic Resonance in Biological Systems, State Key Laboratory of Magnetic Resonance and Atomic and Molecular Physics, Wuhan Centre for Magnetic Resonance, Wuhan Institute of Physics and Mathematics, Chinese Academy of Sciences (CAS), Wuhan 430071, China

[§]Department of Chemistry, The Pennsylvania State University, University Park, Pennsylvania, 16802, USA

[&]Metabolomics Facility, The Huck Institutes of the Life Sciences, The Pennsylvania State University, University Park, Pennsylvania, 16802, USA

Abstract

Environmental exposure to dioxins and dioxin-like compounds poses a significant health risk for human health. Developing a better understanding of the mechanisms of toxicity through activation of the aryl hydrocarbon receptor (AHR) is likely to improve the reliability of risk assessment. In this study, the AHR-dependent metabolic response of mice exposed to 2,3,7,8-tetrachlorodibenzofuran (TCDF) were assessed using global ^{1}H nuclear magnetic resonance (NMR)-based metabolomics and targeted metabolic profiling of extracts obtained from serum and liver. ^{1}H NMR analyses revealed that TCDF exposure suppressed gluconeogenesis and glycogenolysis, stimulated lipogenesis, and triggered inflammatory gene expression in an *Ahr*-dependent manner. Targeted analyses using gas chromatography mass spectrometry showed TCDF treatment altered the ratio of unsaturated/saturated fatty acids. Consistent with this observation, an increase in hepatic expression of *stearoyl coenzyme A desaturase 1* was also observed. In addition, TCDF exposure resulted in inhibition of *de novo* fatty acid biosynthesis manifested by down-regulation of acetyl-CoA, malonyl-CoA and palmitoyl-CoA metabolites and related mRNA levels. In contrast, no significant changes in the levels of glucose and lipid were observed in serum and

[*]To whom correspondence should be addressed. Address: 322 Life Sciences Building, Center for Molecular Toxicology and Carcinogenesis, Department of Veterinary and Biomedical Sciences, The Pennsylvania State University, University Park, PA 16802; USA, Phone: 8148674565; Fax: ; Email: adp117@psu.edu

CONFLICT of INTEREST

All authors have no conflicts to declare.

Supplementary information

Supplementary tables and figures are available via the Internet at http://pubs.acs.org.

liver obtained from *Ahr*-null mice following TCDF treatment, thus strongly supporting the important role of the AHR in mediating the metabolic effects seen following TCDF exposure.

Keywords

Metabolomics; TCDF; Nuclear magnetic resonance (NMR); AHR; Gas and liquid chromatography-mass spectrometry (GC/LC-MS)

INTRODUCTION

2, 3, 7, 8-tetrachlorodibenzofuran (TCDF), 2,3,7,8-tetrachlorodibenzo-p-dioxin (TCDD) and many structurally related halogenated aromatic hydrocarbons (HAHs) and polynuclear aromatic hydrocarbons (PAHs) are environmentally persistent and toxic compounds commonly generated as byproducts of municipal waste combustion.[1] These environmental contaminates can exert diverse biological and toxic effects.[2–4]

The molecular mechanisms of TCDD toxicity have been extensively investigated by a number of microarray analyses[5,6] and metabolomic approaches[7–9] using rodent models. For example, the AHR target gene *TiPARP* has been reported to be associated with suppression of hepatic gluconeogenesis by TCDD and confirmed by decreased expression of phosphoenolpyruvate carboxykinase (*Pepck*), glucokinase (*Gck*), and glucose 6-phosphatase (*G6pase*) genes, which encode for enzymes controlling gluconeogenic flux.[10] Interestingly, TCDD exposure in rats results in tissue-specific differences in the regulation of PEPCK activity including a significant decrease in liver PEPCK activity yet kidney and brown adipose tissue show a significant increase in PEPCK activity.[11] Serum metabolomics revealed that down-regulation of hepatic carboxylesterase 3 was related to an inflammatory cascade involved in steatohepatitis induced by dioxin exposure without activation of the AHR signaling pathway.[8] Aside from hepatoxicity, TCDD-induced immunotoxicity and inflammation has also been shown to be associated with Foxp3+ nTreg cells and their proportional increase in abundance at sites of inflammation through the activation of AHR.[12,13] Hence, a holistic systems approach, facilitated through metabolomics approaches in similar fashion to previously published studies with TCDD, [7–9,50] may be useful to further our understanding of the dynamic metabolic effects of TCDF in vivo.[14–17]

In the current study, we analyzed TCDF-induced changes in serum and liver extracts of wild-type and *Ahr*-null mice using a combination of global ^{1}H NMR and targeted GC/LC-MS based metabolomic approaches. The objectives were to investigate the metabolic responses of mice to TCDF exposure and to further our understanding of the role the AHR plays in mediating the response to these environmental chemicals.

MATERIALS AND METHODS

Chemicals

Sodium chloride, K_2HPO_4 and NaH_2PO_4 (all analytical grade) were obtained from Sigma-Aldrich Chemical Co. Ltd. (St Louis, MO). Sodium 3-trimethylsilyl [2,2,3,3-d_4] propionate

(TSP-d_4) and D_2O (99.9% in D) and 2, 3, 7, 8-tetrachlorodibenzofuran (TCDF, 99.4%) were purchased from Cambridge Isotope Laboratories (Miami, FL).

Animal Experiment and Samples Collection

Animal experimental procedures were performed according to the National Institutes of Health (NIH) guidelines and approved by the Pennsylvania State University Institutional Animal Care and Use Committee. Male C57BL/6J mice (6 weeks old) were purchased from the Jackson Laboratory (Bar Harbor, Maine). A total of 12 mice were housed in temperature- and a light-controlled room and given water and food *ad libitum*. After acclimatization for one week, mice were randomly divided into two groups of six and trained to eat dough pills (Bio-Serve, Frenchtown, NJ) without TCDF for another week. The dough pills with TCDF (acetone solution as vehicle) were prepared with tablet molds and uniformly contained 0.15 μg TCDF for one mouse per pill, thus providing final dosage of 5 μg/kg body weight, respectively. In the TCDF studies, mice were fed with the dough pills containing TCDF continuously for five days (one pill per mouse per day). Male $Ahr^{-/-}$ mice (C57BL/6J congenic mice) were obtained from Dr. Christopher Bradfield (University of Wisconsin, Madison WI) and bred in house. The TCDF dose used in the $Ahr^{-/-}$ mice was 24 μg/kg body weight and the treatment procedure was the same as described above with the dough pills containing TCDF continuously for five days (one pill per mouse per day). Urine and feces were collected every other day (i.e., day 2, 4, and 6) over the TCDF treatment period. Blood, liver and intestinal tissue samples were collected immediately following CO_2 asphyxiation on day 7. All samples were stored at −80 °C until analysis.

Histopathology

Formalin fixed liver tissue was embedded in paraffin wax, sectioned (3–4 μm), and stained with hematoxylin and eosin (H&E) followed with examination under a microscope.

RNA Isolation and Quantitative Gene Expression Analysis

RNA was extracted from frozen liver and ileum tissue (50 mg) using TRIzol reagent (Invitrogen, Carlsbad, CA). After extraction, the concentration of RNA was determined by NanoDrop (ND-1000, V 3.3) and its quality was confirmed by the 260/280 and 260/230 ratios. cDNA was synthesized from 1 μg of total RNA using Superscript II reverse transcriptase (Invitrogen). Gene-specific primers were used in each reaction and all results were normalized to β-*actin* mRNA. Gene expression was performed on an ABI Prism 7900HT Fast Real-Time PCR sequence detection system (Applied Biosystems, Foster City, CA).

Sample Preparation for NMR Spectroscopy

Serum samples were prepared by mixing 200 μL serum with 400 μL saline solution containing 30% D_2O; 550 μL samples was transferred into 5 mm NMR tubes after vortexing and centrifugation (11180 x g, 10 min, 4 °C). Liver tissues (~50 mg) were extracted three times with 600 μL of precooled methanol-water mixture (2/1, v/v) using the PreCellys Tissue Homogenizer (Bertin Technologies, Rockville, MD). After centrifugation at 11180 x g for 10 min at 4 °C, the combined supernatants were dried. Each of the aqueous extracts

was separately reconstituted into 600 μL phosphate buffer (K_2HPO_4/NaH_2PO_4, 0.1 M, pH 7.4, 50% v/v D_2O) containing 0.005% sodium 3-trimethylsilyl [2,2,3,3-d4] propionate (TSP-d_4) as chemical shift reference. Following centrifugation, 550 μL of each extract was transferred into 5 mm NMR tube for NMR analysis.

^{1}H NMR Spectroscopy—^{1}H NMR spectra of serum and aqueous liver extracts were acquired at 298 K on a Bruker Avance III 600 MHz spectrometer (operating at 600.08 MHz for ^{1}H and at 150.93 MHz for ^{13}C) equipped with a Bruker inverse cryogenic probe (Bruker Biospin, Germany). For aqueous liver extracts, typical one-dimensional NMR spectrum was acquired for each of all samples employing the first increment of NOESY pulse sequence (NOESYPR1D). For serum, water-presaturated Carr-Purcell-Meiboom-Gill (CPMG) CPMG pulse sequence (recycle delay-90°-$(\tau$-180°-$\tau)_n$-acquisition) was employed to attenuate NMR signals from macromolecules whereas diffusion-edited spectra can be acquired to obtain only signals of macromolecules such as lipid, lipoprotein and long chain fatty acids. To suppress the water signal, a weak continuous wave irradiation in CPMG method was applied to the water peak during recycle delay (2 s) and mixing time (100 ms). Diffusion-edited spectra were acquired as with diffusion time (Δ) of 200 ms, a duration of the magnetic field pulse gradients (δ) of 1000 us and pulse-field gradient strength of 31.2 G/cm. The 90° pulse length was adjusted to approximately 10 μs for each sample and 64 transients were collected into 32 k data points for each spectrum with spectral width of 20 ppm. To facilitate NMR signal assignments, a range of 2D NMR spectra were acquired and processed for selected samples including ^{1}H-^{1}H correlation spectroscopy (COSY), ^{1}H-^{1}H total correlation spectroscopy (TOCSY), ^{1}H-^{13}C heteronuclear single quantum correlation (HSQC), and ^{1}H-^{13}C heteronuclear multiple bond correlation spectra (HMBC).

Spectral Data Processing and Multivariate Data Analysis

All free induction decays (FID) were multiplied by an exponential function with a 1 Hz line broadening factor prior to Fourier transformation. The spectra were referenced to TSP-d_4 at δ 0.00 when TSP-d_4 was present in liver extracts. Otherwise, the chemical shift of anomeric proton signal of α-glucose (δ 5.233) was used as chemical shift reference for serum. ^{1}H NMR spectra were corrected manually for phase and baseline distortions and spectral region δ 0.50–9.50 was integrated into regions with equal width of 0.004 ppm (2.4 Hz) using AMIX software package (V3.8, Bruker-Biospin). Region δ 4.60–5.15 was discarded by imperfect water saturation. Each bucketed region was then normalized to the total sum of the spectral integrals to compensate for the overall concentration differences prior to statistical data analysis.

Multivariate data analysis was carried out with SIMCAP+ software (version 13.0, Umetrics, Sweden) as described.[32,48] Briefly, Principal Component Analysis (PCA) and Orthogonal Projection to Latent Structures with Discriminant Analysis (OPLS-DA) were conducted on the NMR data. The OPLS-DA models were validated using a 7-fold cross validation method and the quality of the model was described by the parameters R^2X and Q^2 values (Figures 1, 2, 3 and 4).[18] After back-transformation of the loadings generated from the OPLS-DA, color-coded correlation coefficient loading plots (MATLAB, The Mathworks Inc.; Natick, MA) were employed to indicate the significance of the metabolite contribution to the class

separation with a “hot” color (e.g., red) being more significant than a “cold” color (e.g., blue). In this study, a cutoff value of $|r| > 0.707$ ($r > 0.707$ and $r < -0.707$) was chosen for correlation coefficient as significant based on the discrimination significance ($p \leq 0.05$).

Fatty Acid Profiling by GC-MS

Liver tissues (~50 mg) were mixed with 1 mL of methanol-chloroform (2/1, v/v) with addition of 5 μL internal standards (50 μM C15:0 free acid and the methyl ester of C17:0) and then homogenized using the Precellys Tissue Homogenizer (Bertin Technologies, Rockville, MD). After centrifugation (20187 x g, 4 °C) for 15 min, the supernatant was collected. 500 μL saline (0.9 %) was added to the liver extracts and serum (50 μL). After vortexing for 5 min and centrifugation (20187 x g, 4 °C) for 15 min, the mixture was separated into two layers. The solution in the bottom layer was transferred into 10 ml glass tube and dried with nitrogen gas. After adding 1 mL MeOH/HCl (41.5ml/9.7ml) and vortexing for 5 min, the solution was incubated overnight at 60°C. The resultant mixture was combined with 5 mL hexane and 5 mL saline. Following vortexing for 5 min, the top layer was collected and dried down with nitrogen gas. The resultant residues were re-dissolved in 200 μl hexane and then transferred to an autosampler vial for GC-MS analysis. Fatty acid composition was measured on an Agilent 7890A-5975C GC-MS system (Agilent Technologies, Santa Clara, CA). A HP-5MS (Agilent Technologies) capillary column (30 m, 0.25 mm ID, 0.25 μm film thickness) was employed with helium as a carrier gas at flow rate of 1mL/min. Sample injection volume was 0.5 μL with a pressure pulsed split ratio (1:10 split, 10 psi). The injection port and detector temperatures were 230 and 250 °C, respectively. The initial column temperature was 80 °C where it was held for 1 min and then increased to 205 °C at a rate of 20 °C/min, and then increased to 220 °C at a rate of 2 °C/min, and then increased to 310 °C at a rate of 15 °C /min, where it was held for 2 min. Fatty acids were quantified by comparing integrated peak areas following normalization to the internal standards.

Coenzyme A profiling by UPLC-TQS-MS

Targeted analysis of coenzyme A was performed using an Acquity UPLC system coupled to a Waters Xevo TQS MS with a C18 BEH (2.1 × 100 mm, 1.7 μm) UPLC column (All Waters, Milford, MA). The internal standard palmitoyl-$^{13}C_{16}$ coenzyme A was obtained from Sigma-Aldrich. Liver tissues (50 mg) were extracted with 750 μL of methanol containing 1mM EDTA by homogenization and then mixed with 375 μL chloroform with vortexing for 15 sec. Following centrifugation (18000 x g, 4 °C) for 5 min, the top layer was collected. After repeating the above extraction process twice with 500 μl water/methanol/chloroform (45:50:5 v/v/v), the combined supernatants were dried down and later dissolved with 400 μL of 10% aqueous acetonitrile containing internal standard (1.0 μM final concentration of palmitoyl-$^{13}C_{16}$ coenzyme A) by sonication. Following vortex and centrifugation, 300 μL supernatants were transferred to an autosampler vial. Analytes were detected by selected reaction monitoring (SRM) or multiple reactions monitoring (MRM) and quantified by measuring the integrated peak areas, and normalized to the response for palmitoyl-$^{13}C_{16}$. Results were calculated according to individual standard curve established with the response ($area_{analyte}/area_{internal\ std.}$).

Serum lysophosphatidylcholine profiling by UHPLC-QTOF-MS

Serum LPCs were extracted using the Folch method.[51] Briefly, 50 μL serum was mixed with 100 μL chloroform and methanol (2:1 v/v). The samples were incubated at room temperature for 5 min after vortexing. Following centrifugation (18000 x g, 4 °C) for 20 min, the bottom layer was collected and then dried down under a gentle stream of nitrogen gas. The samples were dissolved with 125 μL of solution containing isopropanol, acetonitrile and water (2:1:1 v/v/v). Following vortex and centrifugation, 100 μL supernatants were transferred to an autosampler vial. Samples (5 ul) were separated by reverse phase UHPLC using a Prominence 20 UFLCXR system (Shimadzu, Columbia MD) with a Waters (Milford, MA) CSH C18 column (100mm x 2.1mm 1.7 um particle size) maintained at 55C and a 20 minute aqueous/acetonitrile/isopropanol gradient, at a flow rate of 225 uL/min. Solvent A was 40% water, 60% acetonitrile with 10 mM ammonium formate and 0.1% formic acid, and Solvent B was 90% isopropanol, 10% acetonitrile with 10 mM ammonium formate and 0.1% formic acid. The initial condition were 60% A and 40 % B, increasing to 43% B at 2 min, 50% B at 2.1 min., 54% B at 12 min, 70% B at 12.1 min and 99% B at 18 min., held at 99% B until 20.0 min before returning to the initial conditions. The eluate was delivered into a 5600 (QTOF) TripleTOF using a Duospray™ ion source (all AB Sciex, Framingham, MA).

Data Analysis

All the experimental values are presented as mean ± s.d. Graphical illustrations and statistical analysis were performed with GraphPad Prism version 6.0 (GraphPad). *P*-values < 0.05 were considered significant.

RESULTS

Metabolic Profiling by ^{1}H NMR Analysis

^{1}H NMR spectra of aqueous liver extracts and serum were obtained from vehicle mice and mice treated with TCDF (Figures 1, 2, and 3). The metabolite resonances were assigned on the basis of previous publications[19–21] and confirmed by a range of 2D NMR experiments (Table S1). Liver extracts spectra (Figure 1) were dominated by amino acids, glucose, glycogen, choline-containing metabolites, organic acids, lipid moieties, and nucleoside metabolite signals. Serum CPMG spectra (Figure 2) contained peaks from glucose, amino acids, carboxylic acids such as lactate, fumarate and D-3-hydroxybutyrate (3-HB), and choline-containing metabolites. Serum diffusion-edited spectra (Figure 3) were comprised of lipoproteins, glycoproteins, triglycerides (TG), phospholipids and long chain fatty acids (LCFA).

Dietary TCDF-Induced Metabolic Changes

PCA was initially performed on the normalized NMR data collected from serum and liver extracts to visualize intrinsic similarities/dissimilarities between the samples and for detection of abnormal data points. Comparative OPLS-DA was subsequently conducted between the NMR data from the TCDF-treated and vehicle-treated mice for the different biological matrices. The cross-validated scores plots indicate separations between the

metabolic profiles of vehicle and corresponding TCDF-dosed mice, whereas the OPLS-DA correlation coefficient plots indicate the relative contribution of the metabolites. Here, the model quality indicators (R^2X and Q^2) clearly showed that the metabolite profiles obtained from the different treatment groups were distinctive. These observations were further supported by results from the model evaluation with CV-ANOVA and permutation tests for the models (Figure S1 and Table S2). The metabolites with statistically significant contributions to group discrimination between TCDF-treated and vehicle-treated groups are labeled in the corresponding color-coded coefficient plots (Figure 1C, 2C, and 3C).

Compared with vehicle-treated mice, TCDF exposure resulted in significant alterations of metabolic profiles of liver extracts as illustrated in the cross-validated OPLS-DA coefficient plot (Figure 1C). Dietary TCDF significantly elevated the levels of lipid moieties, unsaturated fatty acid (UFA), and glycogen but significantly decreased the levels of hepatic glucose and lactate. The same OPLS-DA strategy was further applied to the metabolic profiles of serum obtained from TCDF-treated and vehicle-treated mice (Figure 2C, 3C and 4). Compared with the vehicle-treated mice, higher levels of lipid, *N*-acetyl glycoproteins (NAG), *O*-acetyl glycoproteins (OAG), phospholipid and LDL/VLDL and lower levels of alanine, citrate, UFA, phosphocholine (PC) and glycerophosphocholine (GPC) were also observed in the serum of TCDF-treated mice. However, the Q^2 values (0.29, 0.26 and 0.11 for the models of liver, serum with CPMG, and diffusion-edited NMR data, respectively) of the OPLS-DA models of data from liver and serum of $Ahr^{-/-}$ mice revealed no significant differences between the TCDF-treated and control (Figure 4, Table S2).

Targeted fatty acid compositional analysis revealed that TCDF exposure led to significant decreases in saturated fatty acids (C18:0 and C20:0) and elevation of mono-saturated fatty acids (C18:1n9) and polyunsaturated fatty acids (C18:2n6, C20:3n6, C20:3n3 and C20:5n3) in the liver (Figure 5A). A significant decrease in saturated fatty acids (C18:0 and C22:0) and an elevation of polyunsaturated fatty acids (C18:2n6) were also found in the serum of TCDF-treated mice (Figure 5B). TCDF exposure also significantly decreased serum lysophosphatidylcholine (LPC) metabolites including C16:0-LPC, C18:0-LPC, C16:1-LPC, C18:2-LPC, and C20:4-LPC (Figure 5D). In addition, significant decreases of coenzymes including acetyl-CoA, butyryl CoA, malonyl CoA, hexanoyl CoA, myristoyl CoA, palmitoyl CoA and stearoyl CoA together with significant elevation of lineleoyl CoA in the livers of TCDF-treated mice were observed (Figure 6A).

Dietary TCDF Alters Expression Profile of Genes Associated with Lipid and Glucose Metabolic Pathways

In order to monitor the transcriptional (and/or changes in mRNA stability/turnover) responses associated with TCDF treatment, we measured the expression of those genes involved in xenobiotic responses, inflammatory signaling, lipid, and glucose metabolism using QPCR. One of the transcriptional targets of AHR, *Cyp1a1*, which is commonly regarded as the most important marker of xenobiotic response, was found to be significantly induced in the liver and ileum of mice after TCDF exposure (Figures 6B and C). TCDF exposure caused significant increase in gene expression of *stearoyl coenzyme A desaturase-1* (*Scd1*), the key enzyme controlling desaturation of saturated fatty acid, in

TCDF-treated mouse livers (Figure 5C). Significant depletion in the expression of fatty acid synthase (*Fasn*) and acetyl-CoA carboxylase 1 (*Acaca*) mRNAs, encoding important enzymes involved in the process of *de novo* fatty acid biosynthesis, in the livers of TCDF-treated mice was also noted (Figure 5C). Furthermore, dietary TCDF exposure caused significant down-regulation of *G6pase*, *Glut2*, and *Pepck* expression in the liver (Figure 6B), and up-regulation of *Lcn-2*, *Il*-1β, *Tnf*-α and *Saa1* expression in the ileum tissues (Figure 6C) involved in glucose metabolism and inflammatory signaling, respectively.

DISCUSSION

Dioxins and dioxin-like compounds such as TCDD and TCDF exert their toxic effects through activation of the AHR.[22,23] Activation of AHR by these potent agonists leads to a multitude of adverse effects such as liver toxicity and may be associated with the development or exacerbation of obesity.[24,25] The objective of the current study was to investigate the metabolic consequences of TCDF exposure that was not associated with overt liver toxicity. We examined metabolic alterations in serum and liver after 5 days of continuous TCDF exposure in both $Ahr^{+/+}$ and $Ahr^{-/-}$ mice using a global ^{1}H NMR metabolomics approach. The effects of dietary TCDF on fatty acid metabolism and related CoA levels were further investigated by targeted GC/LC-MS analyses. QPCR analyses were also employed to validate the relevant gene expression. The results indicated that TCDF exposure caused comprehensive metabolic alterations in serum and liver, which were found to be AHR-dependent (Figure 7).

Hepatotoxicity Induced by Low TCDF

Based on allometric scaling calculations, the TCDF dose (5 μg/kg body weight) used in this study is equivalent to 600 ng/kg body weight in humans and lower than that used in our previous study (24 μg/kg body weight); however this calculation does not consider total body burden.[48] In this study, liver histopathology showed that dietary TCDF (5 μg/kg body weight) exposure in mice induced mild hepatotoxicity (Figure S2). In addition, dietary TCDF exposure induced significant changes in xenobiotic and energy metabolism based on QPCR and global ^{1}H NMR metabolomic analyses. The metabolic pathway related to AHR activation was altered, manifested by higher expression of *Cyp1a1*, which is involved in the detoxification of xenobiotics in the liver and intestinal tract of TCDF-treated mice. Hepatic cytochromes p450s are useful biomarkers of xenobiotic toxicity and have been widely used to evaluate the toxic effects of environmental pollutants.[26,27,50] Our previous study showed that $Ahr^{-/-}$ mice exhibited no significant change histopathologically and had no change in the liver enzymes ALT, ALP and CYP1A1,[48] suggesting TCDF mediated mild liver injury through activation of AHR. Further, previous study showed that the $Ahr^{-/-}$ mice were relatively unaffected by doses of TCDD (2000 μg/kg) that were tenfold higher than those found to induce severe toxic and pathologic effects in wild-type mice.[52]

The depletion of citrate in serum and fumarate in liver induced by dietary TCDF exposure (Figure 1 and 2) suggests an alteration of TCA cycle (Figure 7), leading to an imbalance of the global energy supply. Citrate and fumarate are important intermediates for the TCA cycle, which is crucial for energy metabolism. Previous studies indicated TCDD-induced

hepatotoxicity was initiated by an inhibition of mitochondrial respiratory function,[28] which inevitably led to changes in the TCA cycle intermediates in the liver and serum profiles. This can also be confirmed by significant depletion of acetyl-CoA level, which is regarded as the "Hub of Metabolism"[29] and is involved in many biochemical reactions, in the liver of TCDF-treated mice. Its main function is to convey the carbon atoms within the acetyl group to the TCA cycle to be oxidized for energy production.[30] Similar observations have been reported in the cases of hepatotoxicity induced by acetaminophen,[31] aflatoxin-B1 (AFB1)[32] and allyl formate.[33] Further, the decrease in alanine levels also indicated perturbations of energy metabolism induced by dietary TCDF.[34]

Lipid Metabolism

The liver is an essential organ in metabolic homeostasis. In the current study, significantly elevated levels of lipid and unsaturated fatty acid (UFA) in the liver of TCDF-treated mice (Figure 1C) indicated hepatic lipogenesis which appears to be a common cellular response to a number of liver toxicants.[31–33] Significant elevation of LDL/VLDL and depletion of HDL, PUFA, and UFA was also observed in the serum of TCDF-treated mice (Figure 3C). The hepatic lipidosis caused by TCDF exposure may also be due to the reduced alterations in lipid transport from the liver to the serum as in the case of the hepatic lipidosis induced by allyl formate,[33] AFB1[32] and methionine.[35] Indeed, markedly decreased expression and activity of Cd36, Apob48, and Apob100 enzymes related to transport of lipid out of the hepatic cells have been observed, in the liver of TCDD-treated rats from previous genomic studies.[36,37] However, no significant changes in the levels of lipoprotein, lipid, and fatty acids were observed in serum between TCDF-treated and vehicle-treated $Ahr^{-/-}$ mice, showing TCDF exposure impacts host lipid export and utilization in an AHR-dependent manner.

GC-MS fatty acid analysis revealed that TCDF-induced disruption in lipid metabolism with a significant elevation in UFA levels and depletion of saturated fatty acids (Figure 5A), indicating a decrease in lipid oxidation with concurrent increases in the biosynthesis of UFAs via desaturation pathways. This implied TCDF-treatment promoted biotransformation from saturated fatty acids to UFA likely via activation of Scd1, which was in agreement with previous observation.[50] TCDF decreased stearate (18:0) and increased oleate (18:1n9) which is consistent with the QPCR results that *Scd1* mRNA levels in TCDF-treated mouse liver were higher than in vehicle-treated mice liver. Additionally, others have reported that TCDD induced the up-regulation of *Elovl5* which plays a key role in elongation of long-chain polyunsaturated fatty acids.[37,38]

TCDF-treatment induced significant depletion in the expression of hepatic *Fasn* and *Acaca* mRNAs, encoding important enzymes involved in the process of *de novo* fatty acid biosynthesis, suggesting that TCDF suppressed *de novo* fatty acid biosynthesis. This was supported by the observation that TCDF induced the down-regulation of acetyl-CoA, palmitoyl CoA, malonyl-CoA, and stearoyl CoA, the key metabolites involved in fatty acid biosynthesis. Consistently, previous studies also indicated TCDD induced inhibition of *de novo* fatty acid biosynthesis and β-oxidation.[39,40] Interestingly, activation of AHR by single injection of β-naphthoflavone (BNF) into mouse and primary human hepatocytes was found

to attenuate the expression of lipogenic genes including *Scd1*, *Acaca*, and *Fasn*), through a DRE-independent mechanism, indicating that AHR plays a key role in the inhibition of fatty acid synthesis in mice and humans.[41]

Serum metabolomics analysis in the present study revealed that dietary TCDF exposure was associated with decreased levels of phosphatidylcholine (PC), glycerolphosphocholine (GPC) (Figure 3C) and lysophosphatidylcholine (LPC) metabolites including C16:0-LPC, C18:0-LPC, C16:1-LPC, C18:2-LPC, and C20:4-LPC (Figure 5D). LPC is a precursor of PC and both PC and GPC are known to be important endogenous compounds associated with bile acid excretion and maintenance of choline homeostasis.[42] Moreover, PC and GPC are not only essential components of cell biomembranes, but also protect cells and their organelles from oxidative stress and lipotoxicity.[43] Our previous study reported that TCDF exposure induced disruption of bile acid excretion such as elevation of tauro-β-muricholate (TβMCA) and deoxycholic acid (DCA).[48] In agreement with our findings, previous investigations reported similar changes in serum metabolites and related mRNA levels including increased expression of hepatic *Lpcat1–4* and *Abcc1/4* and reduced expression of *Slc10a1* and *Slco1a1* in methionine- and choline-deficient diet-induced nonalcoholic steatohepatitis and in GalN-injected *ob/ob* mice models.[44] Collectively, these observations suggested dietary TCDF disrupted cell structural integrity and triggered robust inflammation, which subsequently may lead to steatohepatitis at higher doses.[49]

Glucose and Glycogen Metabolism

Compared with vehicle, mice administered dietary TCDF exhibited significantly reduced glucose and lactate and elevated glycogen levels in liver (Figure 1C), suggesting that one of the consequences of TCDF exposure is inhibition of gluconeogenesis and glycogenolysis. Similar observations have been reported in the case of suppression of hepatic gluconeogenesis by TCDD through the AHR target gene *TiPARP*.[10] Further, such depletion of hepatic glucose has also been observed in human HCC and rats exposed to perfluorododecanoic acid[21] and mycotoxin.[32] Consistently, as reported here, markedly decreased expression of *Pepck*, *G6pase*, and *Glut2*, which encode enzymes important for controlling gluconeogenic flux, in the liver of TCDF-treated mice (Figure 6B). Moreover, a previous microarray study also reported that several enzymes involved in carbohydrate metabolism such as glucokinase (*Gck*) and pyruvate carboxylase (*Pc*) were also down-regulated after TCDD exposure.[5] Taken together, disruption of lipid and carbohydrate metabolism further indicated hepatotoxicity and subsequent perturbations of energy metabolism induced by dietary TCDF exposure.

Gut Responses and Inflammation

Aside from hepatotoxicity, the gastrointestinal tract was affected by dietary TCDF exposure, which was manifested by up-regulation of *Cyp1a1* and *Lcn-2*, *Il*-1β, *Tnf*-α and *Saa1* in the ileum tissues, indicating significant AHR activation and inflammation in the gut (Figure 6C). One possible explanation for these results is that the AHR plays a direct role in the regulation of inflammatory gene expression. This notion is supported by recent studies that have shown that there are functional dioxin response elements in the *Il-6* promoter that are capable of synergistically increasing transcription in the presence of an inflammatory signal

and an AHR ligand.[45] A previous study showed that LCN-2 was a sensitive and dynamic non-invasive biomarker for intestinal inflammation; LCN-2 levels are dramatically increased upon TCDF exposure.[46] In addition, dietary TCDF exposure induced markedly elevated levels of OAG and NAG in serum. High levels of OAG and NAG in mouse serum, which are regarded as “acute-phase” glycoproteins related to inflammation of injured tissue,[47] further confirmed inflammatory conditions in mice after TCDF exposure. Our previous study showed that *Ahr*$^{-/-}$ mice exhibited no significant changes in expression of *Il*-1β and *Tnf*-α, indicating that the inflammation triggered by TCDF was dependent on AHR.[48]

In conclusion, dietary TCDF exposure induced liver dysfunction and significant alterations in several metabolic pathways, including hepatic lipogenesis, perturbed TCA cycle, disrupted carbohydrate and amino acid metabolism as well as inhibition of *de novo* fatty acid biosynthesis (Figure 6). Such dysregulation may also cause gut dysfunction and inflammation. Interestingly, the mild liver injury and the subsequent metabolic disorders induced by TCDF exposure were found to be AHR-dependent. Our results have highlighted that an integrated global ^{1}H NMR and targeted GC/LC-MS analyses of multiple biological matrices provided a systemic method for elucidating mechanisms underlying a toxic insult.

Supplementary Material

Refer to Web version on PubMed Central for supplementary material.

Acknowledgments

This work was supported by National Institute of Environmental Health Sciences [Grants ES004869 (GHP), ES019964 (GHP), and ES022186 (ADP)]. Dr. Limin Zhang is a Penn State Institutes of Energy and the Environment Research Fellow.

REFERENCES

1. Harnly M, Stephens R, McLaughlin C, Marcotte J, Petreas M, Goldman L. Polychlorinated Dibenzo-p-dioxin and Dibenzofuran Contamination at Metal Recovery Facilities, Open Burn Sites, and a Railroad Car Incineration Facility. Environ. Sci. Technol. 1995; 29(3):677–684. [PubMed: 22200276]
2. Peters JM, Narotsky MG, Elizondo G, Fernandez-Salguero PM, Gonzalez FJ, Abbott BD. Amelioration of TCDD-induced teratogenesis in aryl hydrocarbon receptor (AhR)-null mice. Toxicol. Sci. 1999; 47(1):86–92. [PubMed: 10048156]
3. Pohjanvirta R, Tuomisto J. Short-term toxicity of 2,3,7,8-tetrachlorodibenzo-p-dioxin in laboratory animals: effects, mechanisms, and animal models. Pharmacol. Rev. 1994; 46(4):483–549. [PubMed: 7899475]
4. Salavaggione OE, Yang C, Kidd LB, Thomae BA, Pankratz VS, Trepanier LA, Weinshilboum RM. Cat red blood cell thiopurine S-methyltransferase: companion animal pharmacogenetics. J. Pharm. Exp. Ther. 2004; 308(2):617–626.
5. Fletcher N, Wahlstrom D, Lundberg R, Nilsson CB, Nilsson KC, Stockling K, Hellmold H, Hakansson H. 2,3,7,8-Tetrachlorodibenzo-p-dioxin (TCDD) alters the mRNA expression of critical genes associated with cholesterol metabolism, bile acid biosynthesis, and bile transport in rat liver: a microarray study. Toxicol. Appl. Pharmacol. 2005; 207(1):1–24. [PubMed: 16054898]
6. Hanlon PR, Zheng W, Ko AY, Jefcoate CR. Identification of novel TCDD-regulated genes by microarray analysis. Toxicol. Appl. Pharmacol. 2005; 202(3):215–2128. [PubMed: 15667827]

7. Lin S, Yang Z, Liu H, Cai Z. Metabolomic analysis of liver and skeletal muscle tissues in C57BL/6J and DBA/2J mice exposed to 2,3,7,8-tetrachlorodibenzo-p-dioxin. Mol. Biosyst. 2011; 7(6):1956–1965. [PubMed: 21465055]
8. Matsubara T, Tanaka N, Krausz KW, Manna SK, Kang DW, Anderson ER, Luecke H, Patterson AD, Shah YM, Gonzalez FJ. Metabolomics identifies an inflammatory cascade involved in dioxin- and diet-induced steatohepatitis. Cell Metab. 2012; 16(5):634–644. [PubMed: 23140643]
9. O'Kane AA, Chevallier OP, Graham SF, Elliott CT, Mooney MH. Metabolomic profiling of in vivo plasma responses to dioxin-associated dietary contaminant exposure in rats: implications for identification of sources of animal and human exposure. Environ. Sci. Technol. 2013; 47(10):5409–5418. [PubMed: 23586690]
10. Diani-Moore S, Ram P, Li X, Mondal P, Youn DY, Sauve AA, Rifkind AB. Identification of the aryl hydrocarbon receptor target gene TiPARP as a mediator of suppression of hepatic gluconeogenesis by 2,3,7,8-tetrachlorodibenzo-p-dioxin and of nicotinamide as a corrective agent for this effect. J. Biol. Chem. 2010; 285(50):38801–38810. [PubMed: 20876576]
11. Viluksela M, Stahl BU, Rozman KK. Tissue-specific effects of 2,3,7,8-Tetrachlorodibenzo-p-dioxin (TCDD) on the activity of phosphoenolpyruvate carboxykinase (PEPCK) in rats. Toxicol. Appl. Pharmacol. 1995; 135(2):308–315. [PubMed: 8545841]
12. Gandhi R, Kumar D, Burns EJ, Nadeau M, Dake B, Laroni A, Kozoriz D, Weiner HL, Quintana FJ. Activation of the aryl hydrocarbon receptor induces human type 1 regulatory T cell-like and Foxp3(+) regulatory T cells. Nat. Immunol. 2010; 11(9):846–853. [PubMed: 20676092]
13. Apetoh L, Quintana FJ, Pot C, Joller N, Xiao S, Kumar D, Burns EJ, Sherr DH, Weiner HL, Kuchroo VK. The aryl hydrocarbon receptor interacts with c-Maf to promote the differentiation of type 1 regulatory T cells induced by IL-27. Nat. Immunol. 2010; 11(9):854–861. [PubMed: 20676095]
14. Ebbels TM, Keun HC, Beckonert OP, Bollard ME, Lindon JC, Holmes E, Nicholson JK. Prediction and classification of drug toxicity using probabilistic modeling of temporal metabolic data: the consortium on metabonomic toxicology screening approach. J. Proteome Res. 2007; 6(11):4407–4422. [PubMed: 17915905]
15. Huang C, Lei H, Zhao X, Tang H, Wang Y. Metabolic influence of acute cyadox exposure on Kunming mice. J. Proteome Res. 2013; 12(1):537–545. [PubMed: 23234330]
16. Waters NJ, Holmes E, Williams A, Waterfield CJ, Farrant RD, Nicholson JK. NMR and pattern recognition studies on the time-related metabolic effects of alpha-naphthylisothiocyanate on liver, urine, and plasma in the rat: an integrative metabonomic approach. Chem. Res. Toxicol. 2001; 14(10):1401–1412. [PubMed: 11599932]
17. Zhao XJ, Hao F, Huang C, Rantalainen M, Lei H, Tang H, Wang Y. Systems responses of rats to mequindox revealed by metabolic and transcriptomic profiling. J. Proteome Res. 2012; 11(9):4712–4721. [PubMed: 22845897]
18. Eriksson L, Andersson PL, Johansson E, Tysklind M. Megavariate analysis of environmental QSAR data. Part II-investigating very complex problem formulations using hierarchical, non-linear and batch-wise extensions of PCA and PLS. Mol. Divers. 2006; 10(2):187–205. [PubMed: 16802062]
19. Fan TW, Colmer TD, Lane AN, Higashi RM. Determination of metabolites by 1H NMR and GC: analysis for organic osmolytes in crude tissue extracts. Anal. Chem. 1993; 214(1):260–271.
20. Dai H, Xiao C, Liu H, Tang H. Combined NMR and LC-MS analysis reveals the metabonomic changes in Salvia miltiorrhiza Bunge induced by water depletion. J. Proteome Res. 2010; 9(3):1460–1475. [PubMed: 20044832]
21. Ding L, Hao F, Shi Z, Wang Y, Zhang H, Tang H, Dai J. Systems biological responses to chronic perfluorododecanoic acid exposure by integrated metabonomic and transcriptomic studies. J. Proteome Res. 2009; 8(6):2882–2891. [PubMed: 19378957]
22. Preeti R, Craig M, Gary HP. Role of the aryl hydrocarbon receptor in drug metabolism. Expert Opin. Drug Metab. Toxicol. 2005; 1(1):1–13. [PubMed: 16922647]
23. Mimura J, Fujii KY. Functional role of AhR in the expression of toxic effects by TCDD. Biochim. Biophys. Acta. 2003; 1619(3):263–268. [PubMed: 12573486]

24. Arsenescu V, Arsenescu RI, King V, Swanson H, Cassis LA. Polychlorinated biphenyl-77 induces adipocyte differentiation and proinflammatory adipokines and promotes obesity and atherosclerosis. Environ. Health Perspect. 2008; 116(6):761–768. [PubMed: 18560532]
25. Wahlang B, Falkner KC, Gregory B, Ansert D, Young D, Conklin DJ, Bhatnagar A, McClain CJ, Cave M. Polychlorinated biphenyl 153 is a diet-dependent obesogen that worsens nonalcoholic fatty liver disease in male C57BL6/J mice. J. Nutr. Biochem. 2013; 24(9):1587–1595. [PubMed: 23618531]
26. Lee HS, Yang M. Applications of CYP-450 expression for biomonitoring in environmental health. Environ. Health Prev. Med. 2008; 13(2):84–93. [PubMed: 19568886]
27. Yi B, Yang JY, Yang M. Past and future applications of CYP450-genetic polymorphisms for biomonitoring of environmental toxicants. J. Environ. Sci. Health. 2007; 25(4):353–377.
28. Labitzke EM, Diani-Moore S, Rifkind AB. Mitochondrial P450-dependent arachidonic acid metabolism by TCDD-induced hepatic CYP1A5; conversion of EETs to DHETs by mitochondrial soluble epoxide hydrolase. Arch. Biochem. Biophys. 2007; 468(1):70–81. [PubMed: 17959137]
29. Filipp FV, Scott DA, Ronai ZA, Osterman AL, Smith JW. Reverse TCA cycle flux through isocitrate dehydrogenases 1 and 2 is required for lipogenesis in hypoxic melanoma cells. Pigment Cell Melanoma Res. 2012; 25(3):375–383. [PubMed: 22360810]
30. Liu Y, He J, Ji S, Wang Q, Pu H, Jiang T, Meng L, Yang X, Ji J. Comparative studies of early liver dysfunction in senescence-accelerated mouse using mitochondrial proteomics approaches. Mol. Cell. Proteomics. 2008; 7(9):1737–1747. [PubMed: 18515266]
31. Coen M, Lenz EM, Nicholson JK, Wilson ID, Pognan F, Lindon JC. An integrated metabonomic investigation of acetaminophen toxicity in the mouse using NMR spectroscopy. Chem. Res. Toxicol. 2003; 16(3):295–303. [PubMed: 12641429]
32. Zhang L, Ye Y, An Y, Tian Y, Wang Y, Tang H. Systems responses of rats to aflatoxin B1 exposure revealed with metabonomic changes in multiple biological matrices. J. Proteome Res. 2011; 10(2): 614–623. [PubMed: 21080729]
33. Yap IK, Clayton TA, Tang H, Everett JR, Hanton G, Provost JP, Le Net JL, Charuel C, Lindon JC, Nicholson JK. An integrated metabonomic approach to describe temporal metabolic disregulation induced in the rat by the model hepatotoxin allyl formate. J. Proteome Res. 2006; 5(10):2675–2684. [PubMed: 17022638]
34. Yang RD, Matthews DE, Bier DM, Wen ZM, Young VR. Response of alanine metabolism in humans to manipulation of dietary protein and energy intakes. Am. J. Physiol. 1986; 250(1):E39–E46. [PubMed: 3942211]
35. Skordi E, Yap IK, Claus SP, Martin FP, Cloarec O, Lindberg J, Schuppe-Koistinen I, Holmes E, Nicholson JK. Analysis of time-related metabolic fluctuations induced by ethionine in the rat. J. Proteome Res. 2007; 6(12):4572–4581. [PubMed: 17966971]
36. Lee JH, Wada T, Febbraio M, He J, Matsubara T, Lee MJ, Gonzalez FJ, Xie W. A novel role for the dioxin receptor in fatty acid metabolism and hepatic steatosis. Gastroenterology. 2010; 139(2): 653–663. [PubMed: 20303349]
37. Angrish MM, Dominici CY, Zacharewski TR. TCDD-elicited effects on liver, serum, and adipose lipid composition in C57BL/6 mice. Toxicol. Sci. 2013; 131(1):108–115. [PubMed: 22977169]
38. Angrish MM, Jones AD, Harkema JR, Zacharewski TR. Aryl hydrocarbon receptor-mediated induction of Stearoyl-CoA desaturase 1 alters hepatic fatty acid composition in TCDD-elicited steatosis. Toxicol. Sci. 2011; 124(2):299–310. [PubMed: 21890736]
39. Lee HG, Yang JH. PKC-delta mediates TCDD-induced apoptosis of chondrocyte in ROS-dependent manner. Chemosphere. 2010; 81(8):1039–1044. [PubMed: 20846705]
40. Lakshman MR, Campbell BS, Chirtel SJ, Ekarohita N. Effects of 2,3,7,8-tetrachlorodibenzo-p-dioxin (TCDD) on de novo fatty acid and cholesterol synthesis in the rat. Lipids. 1988; 23(9):904–906. [PubMed: 3185127]
41. Tanos R, Murray IA, Smith PB, Patterson A, Perdew GH. Role of the Ah receptor in homeostatic control of fatty acid synthesis in the liver. Toxicol. Sci. 2012; 129(2):372–379. [PubMed: 22696238]
42. Li Z, Vance DE. Phosphatidylcholine and choline homeostasis. J. Lipid Res. 2008; 49(6):1187–1194. [PubMed: 18204095]

43. Han MS, Park SY, Shinzawa K, Kim S, Chung KW, Lee JH, Kwon CH, Lee KW, Lee JH, Park CK, Chung WJ, Hwang JS, Yan JJ, Song DK, Tsujimoto Y, Lee MS. Lysophosphatidylcholine as a death effector in the lipoapoptosis of hepatocytes. J. Lipid Res. 2008; 49(1):84–97. [PubMed: 17951222]
44. Tanaka N, Matsubara T, Krausz KW, Patterson AD, Gonzalez FJ. Disruption of phospholipid and bile acid homeostasis in mice with nonalcoholic steatohepatitis. Hepatology. 2012; 56(1):118–129. [PubMed: 22290395]
45. Brett CD, Jennifer CS, Lauren JF, Ann K, Gar HP. Mechanistic insights into the events that lead to synergistic induction of interleukin 6 transcription upon activation of the aryl hydrocarbon receptor and inflammatory signaling. J. Biol. Chem. 2010; 285(32):24388–24397. [PubMed: 20511231]
46. Benoit C, Gayathri S, Maria AD, Andrew NY, Andrew TG, Matam V-K. Fecal lipocalin 2, a sensitive and broadly dynamic non-invasive biomarker for intestinal inflammation. 2012; 7(9):e44328.
47. Grootveld M, Claxson AW, Chander CL, Haycock P, Blake DR, Hawkes GE. High resolution proton NMR investigations of rat blood plasma: assignment of resonances for the molecular mobile carbohydrate side-chains of acute-phase glycoproteins. FEBS Lett. 1993; 322(3):266–276. [PubMed: 7683613]
48. Zhang, L.; Nichols, RG.; Correll, J.; Murray, IA.; Tanaka, N.; Smith, P.; Hubbard, TD.; Sebastian, A.; Albert, I.; Hatzakis, E.; Gonzalez, FJ.; Perdew, GH.; Patterson, AD. Effects of aryl hydrocarbon receptor activation by persistent organic pollutants on gut microbiota-host metabolic homeostasis in mice. Environ. Health Perspect. 2015. http://ehp.niehs.nih.gov/1409055/
49. Matsubara T, Tanaka N, Krausz KW, Manna SK, Kang DW, Anderson ER, Luecke H, Patterson AD, Shah YM, Gonzalez FJ. Metabolomics identifies an inflammatory cascade involved in dioxin- and diet-induced steatohepatitis. Cell Metab. 2012; 16(5):634–644. [PubMed: 23140643]
50. Forgacs AL, Michael NK, Meghan KM, Bryan M, Nicholas D, Gary LJ, Lyle DB, Timothy RZ, Nicholas VR. Comparative metabolomic and genomic analyses of TCDD-elicited metabolic disruption in mouse and rat liver. Toxicol. Sci. 2012; 125(1):41–55. [PubMed: 21964420]
51. Folch J, Lees M, Sloane SG. A simple method for the isolation and purification of total lipides from animal tissues. J. Biol. Chem. 1957; 226(1):497–509. [PubMed: 13428781]
52. Fernandez-Salgueroa PM, David MH, Stuart R, Jerrold MW, Gonzalez FJ. Aryl-hydrocarbon receptor-deficient mice are resistant to 2,3,7,8-Tetrachlorodibenzo-p-dioxin-induced toxicity. Toxicol. Appl. Pharmacol. 1996; 140(1):173–179. [PubMed: 8806883]

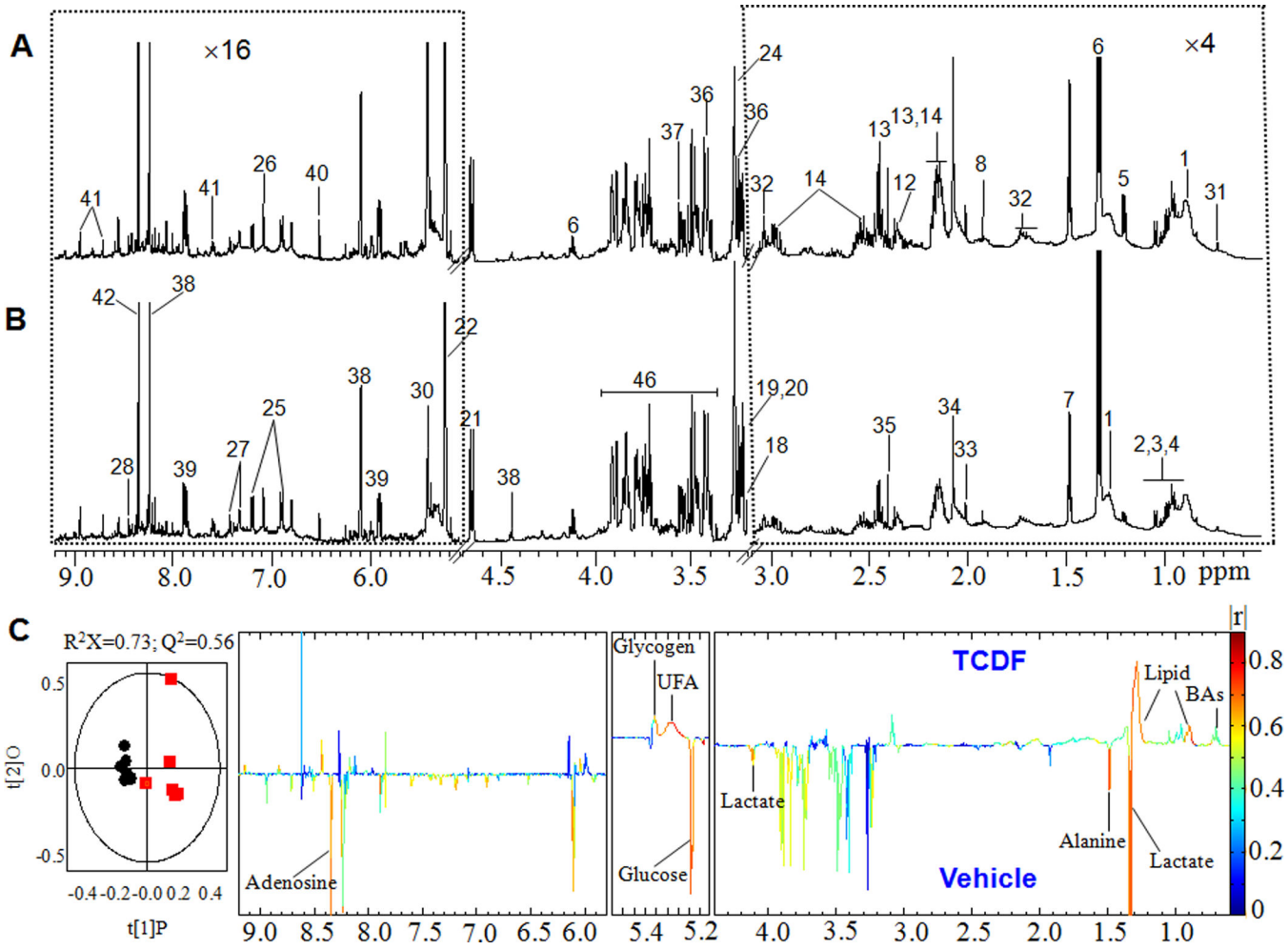

Figure 1.

Representative 600 MHz ^{1}H NMR spectra of liver extracts from the vehicle (A) and TCDF-treated mice (B). The regions of δ 6.10–9.20 and δ 0.60–3.10 in the liver spectra was vertically expanded 16 times and 4 times compared with the region of δ 3.10–4.70, respectively. O-PLS-DA scores (left) and coefficient-coded loadings plots (right) for the models obtained from the NMR data of liver aqueous extracts (C). The model was cross-validated with CV-ANOVA, $p = 2.33 \times 10^{-3}$ corresponding to liver extracts of mice after vehicle and TCDF exposure. Metabolite assignments are shown in Figure 1 and Table S1.

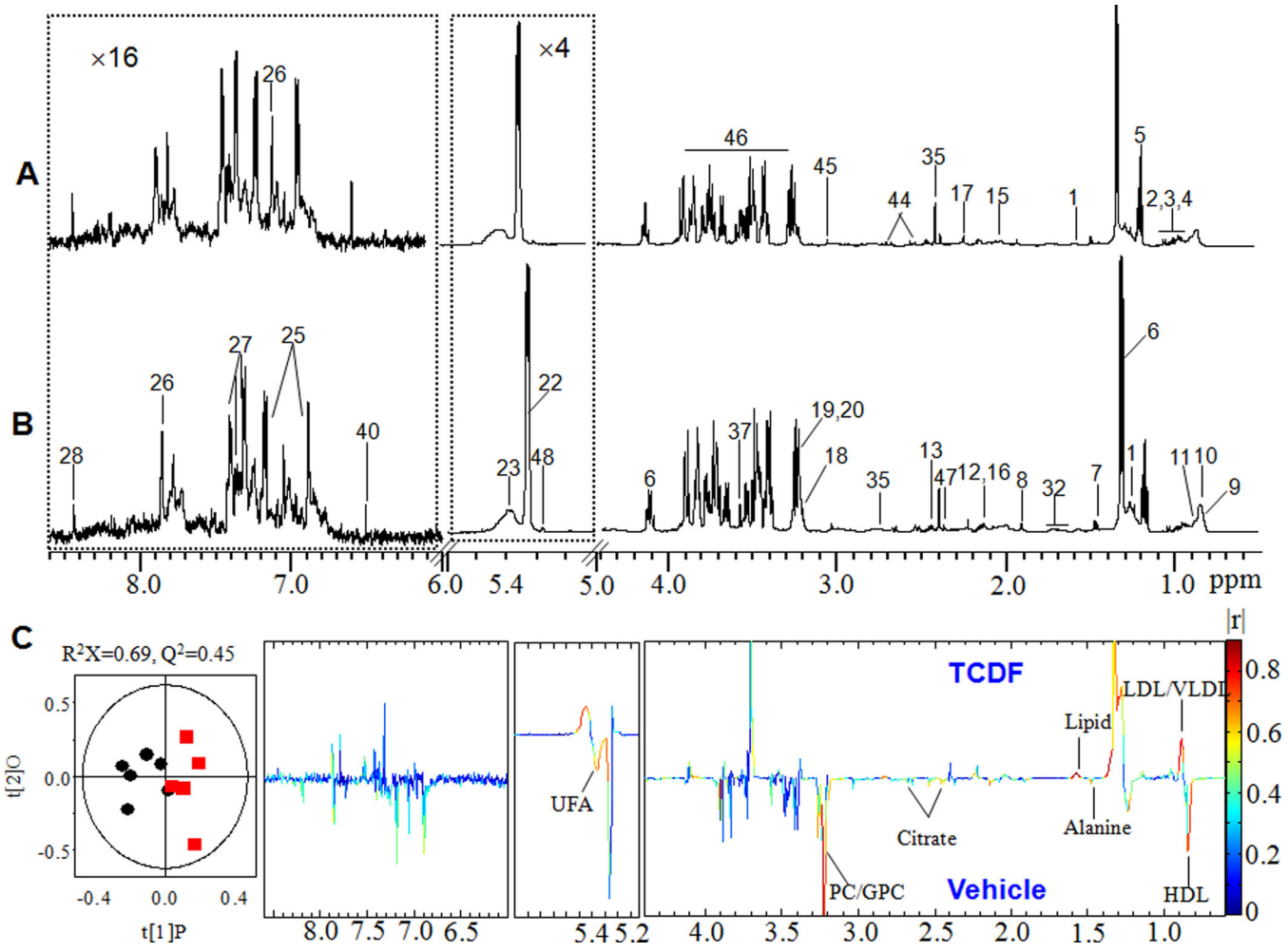

Figure 2.

Representative 600 MHz ^{1}H NMR CPMG spectra of serum from the vehicle (A) and TCDF-treated mice (B). The regions of δ 6.00–8.50 and δ 5.00–5.50 in the liver spectra was vertically expanded 16 times and 4 times compared with the region of δ 0.50–4.40, respectively. O-PLS-DA scores (left) and coefficient-coded loadings plots (right) for the models obtained from the NMR data (C). The model was cross-validated with CV-ANOVA, $p = 0.035$ corresponding to serum of mice after vehicle and TCDF exposure, respectively. Metabolite keys are shown in Figure 2 and Table S1.

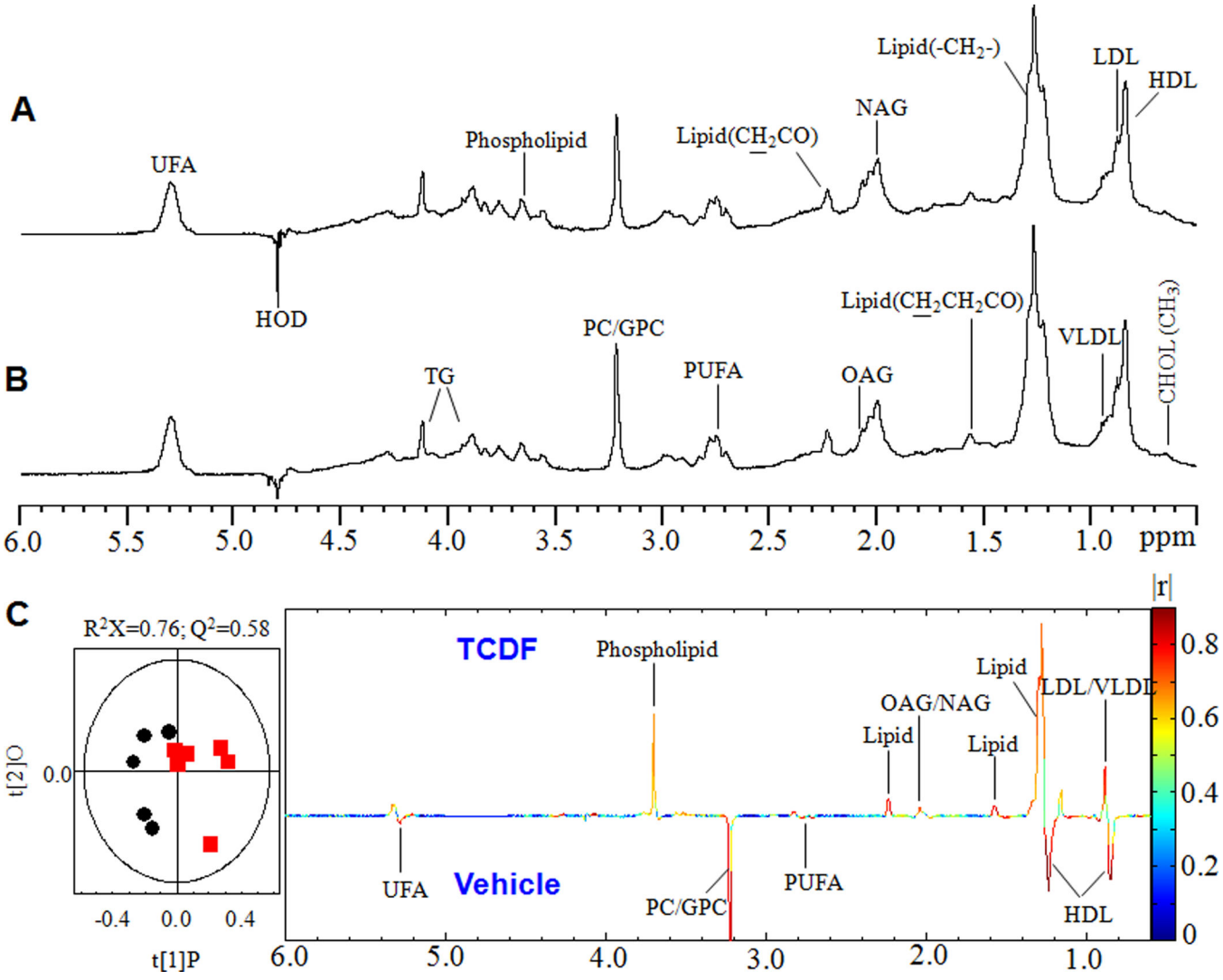

Figure 3.

Representative 600 MHz ^{1}H NMR diffusion-edited spectra of serum from vehicle (A) and TCDF-treated mice (B) and O-PLS-DA scores (left) and coefficient-coded loadings plots (right) for the models obtained from the NMR data (C). The model was cross-validated with CV-ANOVA, $p = 2.06 \times 10^{-3}$ corresponding to serum of mice after vehicle and TCDF exposure, respectively. Metabolite keys are shown in Figure 3 and Table S1.

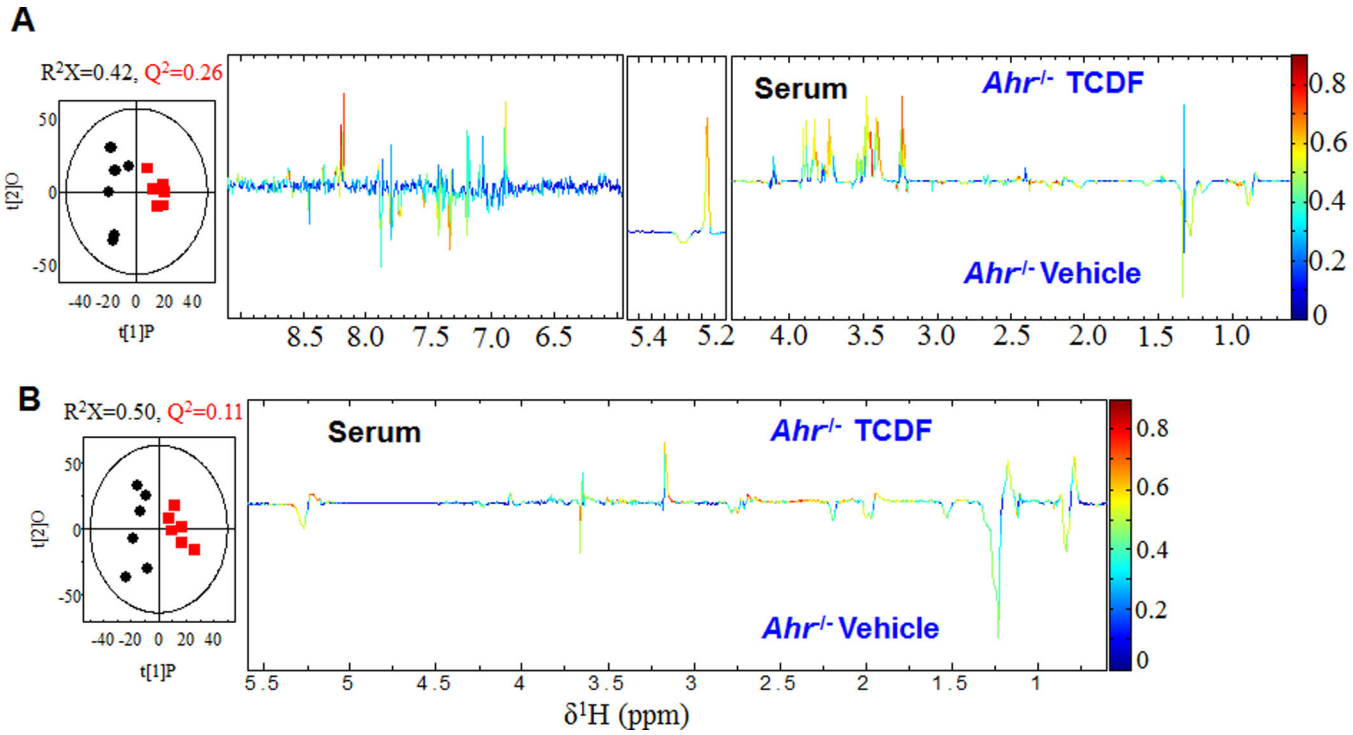

Figure 4.

O-PLS-DA scores (left) and coefficient-coded loadings plots (right) for the models obtained from the CPMG (A) and diffusion-edited (B) NMR data acquired from serum of $Ahr^{-/-}$ control and TCDF-treated $Ahr^{-/-}$ mice. The model was cross-validated with CV-ANOVA, $p = 0.571$ and 1.392 corresponding to serum of $Ahr^{-/-}$ mice after vehicle and TCDF exposure, respectively. Metabolite keys are shown in Figure 3 and Table S1.

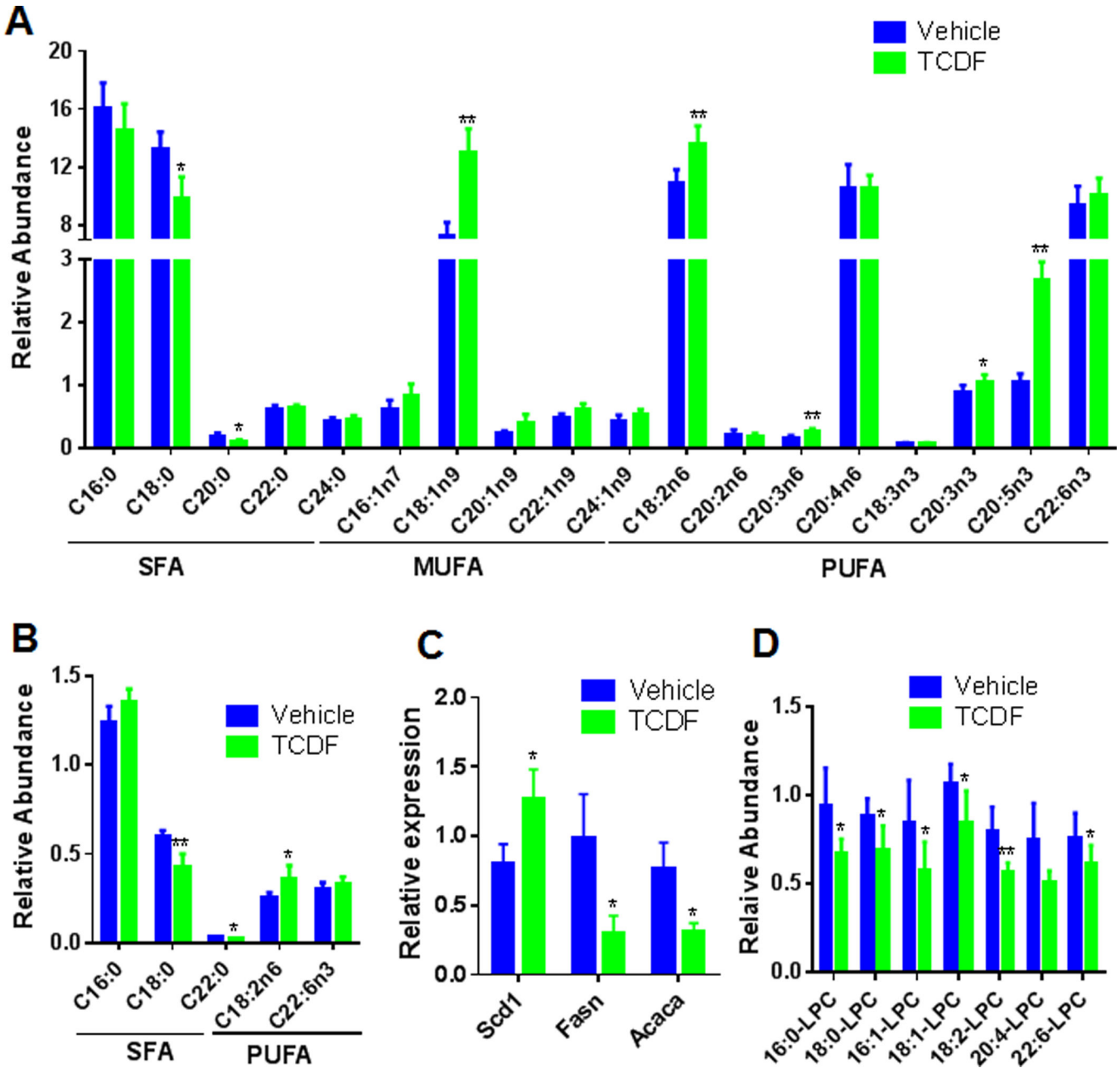

Figure 5.

Fatty acid composition in liver (A) and serum (B) of vehicle-treated (blue bars) and 5 μg/kg TCDF-treated mice (green bars). Fatty acids were extracted by the Folch method and quantified by GC-MS. QPCR analysis of *Scd1, Fasn* and *Acaca* mRNA expression in the liver (C) and lysophosphatidylcholine (LPC) composition in serum (D) by LC-MS. The primers used in this study are listed in Table S2. Data are presented as mean ± s. d, n = 6 per group; *p < 0.05, **p < 0.01, ***p < 0.001, two-tailed Student's t-test.

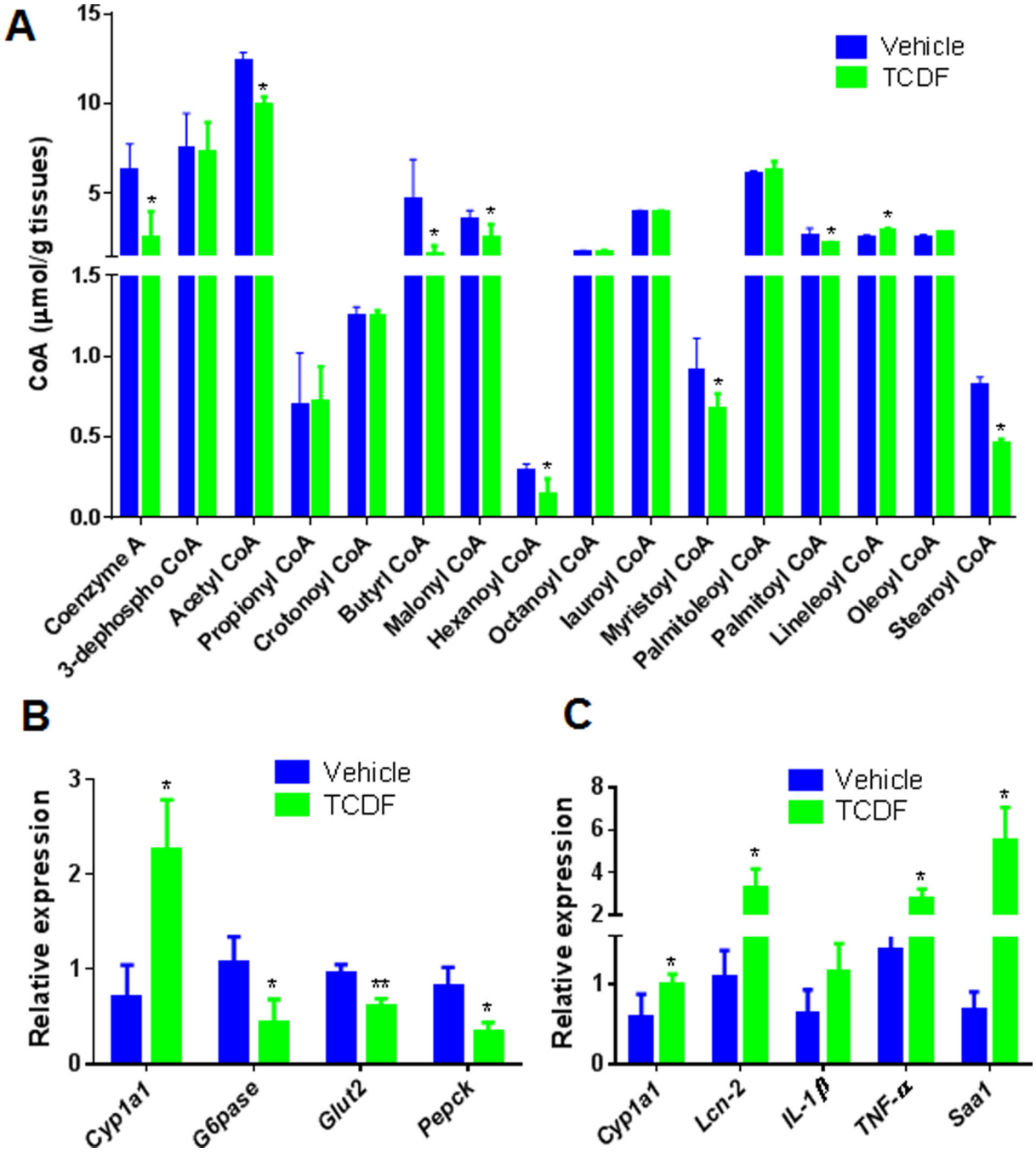

Figure 6.

Coenzymes CoA composition in liver (A) from vehicle-treated (blue bars) and 5 μg/kg TCDF-treated mice (green bars). QPCR analysis of mRNA levels of *Cyp1a1, G6pase, Glut2* and *Pepck* in the liver (B) and inflammatory cytokine (*Lcn-2, IL-1β, TNF-α* and *Saa1*) expression in the ileum (C). The primers used in this study are listed in Table S2. Data are presented as mean ± s. d., n = 6 per group; *$p < 0.05$, **$p < 0.01$, ***$p < 0.001$, two-tailed Student's *t*-test.

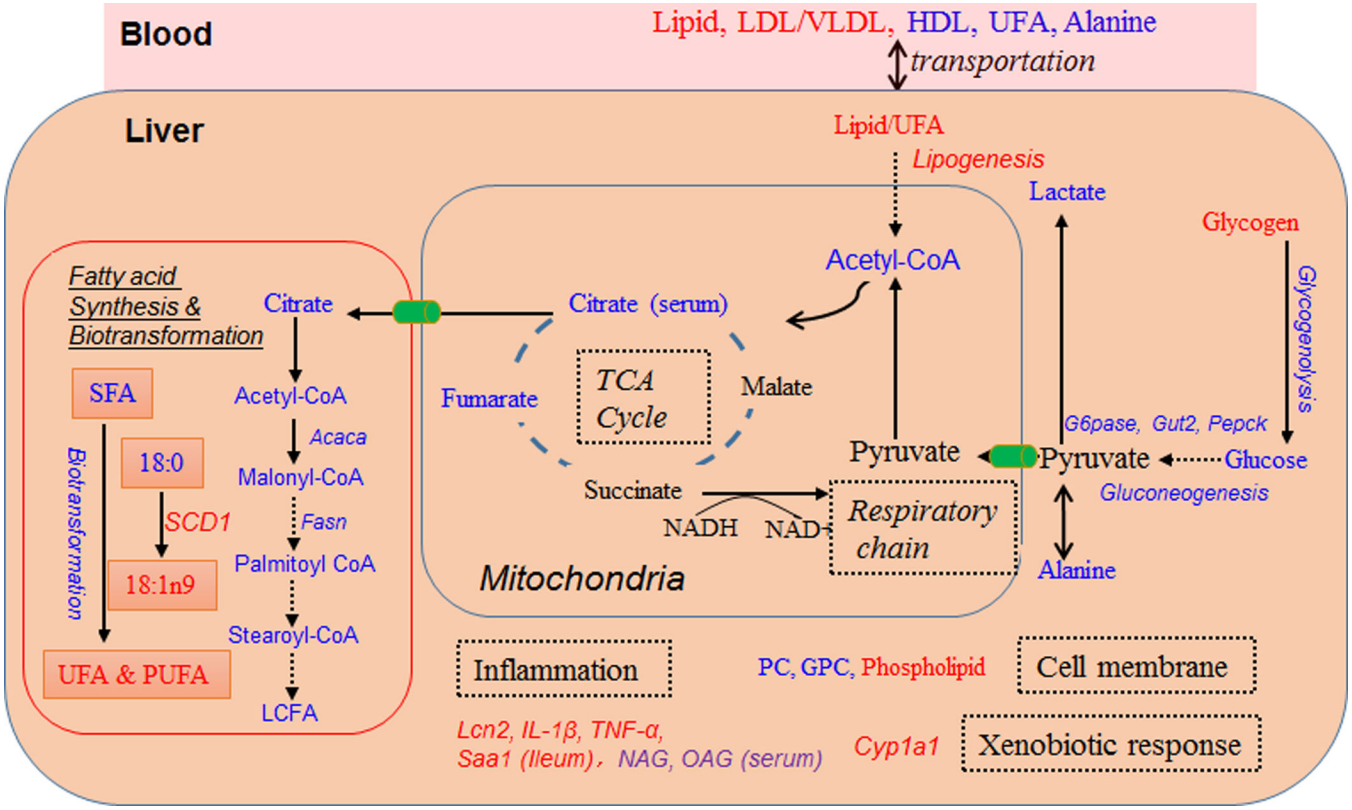

Figure 7.

A summary of the significant changes found in the host metabolome of mice exposed to TCDF. Dietary TCDF altered many metabolic pathways involved in hepatic lipogenesis, gluconeogenesis, glycogenolysis, TCA cycle, amino acids, and lipid metabolism and inflammatory signaling pathways. The metabolites or mRNAs in red or blue represent a higher or lower level in the respective biological matrices (liver and serum) obtained from TCDF-treated mice compared to vehicle.